# Nanosatellite clusters for multi-spectral, bi-directional reflectance distribution function estimations

Sreeja Nag[1,2,3], Charles Gatebe[2,3], Olivier de Weck[1]
[1]*Massachusetts Institute of Technology, Cambridge, MA 02139, USA*
[2]*NASA Goddard Space Flight Center, 8800 Greenbelt Road, Greenbelt, MD 20771, USA*
[3]*Universities Space Research Association, 10211 Wincopin Circle, Columbia, MD 21044, USA*
*Email:* sreeja_n@mit.edu

The bidirectional reflectance distribution function (BRDF) of any pixel on the Earth's surface describes its physical structure and composition. BRDF is important for calculating radiative forcing in clouds and determinant of the energy balance through the atmosphere, and sequentially climate change. Although BRDF cannot be measured directly, it can be estimated using models of surface scattering and reflectance data acquired at different sensor viewing angles, sun illumination angles and spectral bands. While many space- based missions have attempted BRDF estimations using forward-aft or cross-scan angular measurements using the same satellite, there has never been a dedicated BRDF mission. This paper introduces the concept of using one or many clusters of nanosatellites in formation flight to make multi-spectral reflectance measurements of a spot on the ground at different zenith and azimuthal angles at the same time by pointing their sensors to the target at the same time. The cluster geometries that have been identified, but are not restricted to, are: strong of pearls configuration, cross track scanning, free orbit ellipses and relative analemmas and metrics of performance – angles, footprint area and attitude control requirements – have been compared. Sun-synchronous low earth orbits as well as equatorial orbits have been identified as orbit preferences for the clusters to achieve global coverage, and pros and cons of each compared. Finally, the proposed nanosatellite constellation design is benchmarked with respect to available nanosatellite subsystems, payload and potential advantages highlighted over past and current missions with BRDF products.

**Key Words:** BRDF, Nanosatellite, Formation Flight

## 1. Introduction

The high need for Earth observation (EO) missions is seen from the increased international collaboration among nation in the field. The rapid need for the development and operational EO systems has led to increased interest in small satellite technologies because it brings spaceborne observation within the reach of every country and gives them the ability to utilize the data at low costs and build application driven missions [1]. NASA has been planning nano and micro satellite based EO programs through the Global Precipitation Measurement (GPM) Constellation, Leonardo-BRDF, GPS Occultation Constellation, Magnetospheric Constellation and Global ITM Constellation, mostly under the NASA New Millenium program for new space technology development which was shelved in 2009 due to Congressional budget cuts. Examples of realized small EO satellite initiatives in the USA have been SAMPEX, FAST, TRACE, SWAS and WIRE, however none of these have been nanosatellites. ESA released its interests in the earth observation nearly 20 years ago through the METOP and Envisat missions, however most of these are huge bus-like satellites[2]. More recently, due to growing commercialization of space in Europe, miniaturization of power systems, ADCS and communication systems and technology transfer programs in the rest of the world, many countries have come up with great small satellite programs of their own. For more than the last decade, universities have taken the lead on cubesats (e.g. CalPoly standards) and nanosat demonstrations (e.g. MIT SPHERES). These small satellites can easily launch as ESPA-class payloads (ESPA = EELV Secondary Payload Adapter, EELV = Evolved Expendable Launch Vehicle) and thus take advantage of cheap piggyback rides on large launch vehicles such as the Atlas V and Delta IV.

Small satellites can be classified into pico, nano, micro, mini satellites; the focus of this paper is on nanosatellites i.e. satellites weighing 10 kg or less with a development time of a little over a year and cost of ~USD $1 million [13]. The advantages of using nanosats are more frequent mission opportunities, larger variety affordable, rapid expansion of the knowledge base and quick scheduling and greater involvement of local and small industries. While cubesats and nanosats have typically been used for technology demonstration by small industry or educational initiatives by universities, literature points at their little utilization for real earth observation science [4]. Some exceptions have been the QuakeSAT by Stanford studying ULF magnetic signals, SwissCube-1 from Lausanne studying the oxygen emission bands from the upper atmosphere, Aalto-1 from Finland and MicroMAS from MIT/Lincoln Labs conducting hyperspectral remote sensing and CanX-2 from Canada for studying GNSS radio occultations.

The time and cost advantages of nanosats may also be put to further use, by the economies of scale, to manufacture many individual modules and create clusters of nanosats (i.e. formation flying within a locality), constellations (i.e. no restriction of relative position or active control required) and clustellations (i.e. constellations of clusters). All the above are grouped under the category of distributed satellite systems which provide the advantages of increased time resolution, multiple angle measurement thus increased performance, easy replacement of a failed or damaged satellite and graceful degradation of performance thus decreased risk of critical system failure. Studying the potential of nanosatellite constellations to combine the temporal resolution of GEO with the spatial resolution of LEO, as documented in literature above at lower costs, risk and schedule , but rarely flown as science missions, we decided to study their applicability for our mission science – as highlighted in the next section.

## 2. Mission Science: Full BRDF Estimation

Our mission science to perform measurements for the estimation of full bidirectional reflectance distribution function (BRDF) of sampled ground points. BRDF describes the properties of anisotropically scattering surfaces in the reflection of solar incident light [5]. It provides a way of geometrically and quantitatively expressing the connection between radiance reflected from a ground pixel in a given direction and the incident irradiance arriving at that pixel from some other direction. BRDF is needed for correction of view angle and illumination angles in image standardization, derivation of surface albedo, climate modeling and the calculation of radiative forcing about clouds, land cover classification, cloud detection and atmospheric corrections [5]. BRDF measurements further promise data products such as albedo, thermal anisotropy, Normalized Difference Vegetation Index (NDVI), aerosol optical properties, land surface temperature and leaf area index (LAI) [6]. Furthermore, it is important to measure them on a low enough time and spatial scale so that instantaneous flux can be correlated with specific phenomena such as hurricanes, fires, El Nino, etc [7]. Figure 1 shows the typical BRDF measurement geometry. Since BRDF measurements require measurement of radiance from multiple angles at the same time from the same ground pixel is impossible to do it through the same satellite. The conflict between what we want and what we can get using a monolith is further expressed in Figure 2. Therefore, the best (and in fact, the only way) of measuring radiance in order to determine BRDF is through the use of multiple satellites i.e. a distributed satellite system. This further strengthens the argument for the use of nanosatellite clusters for our mission science.

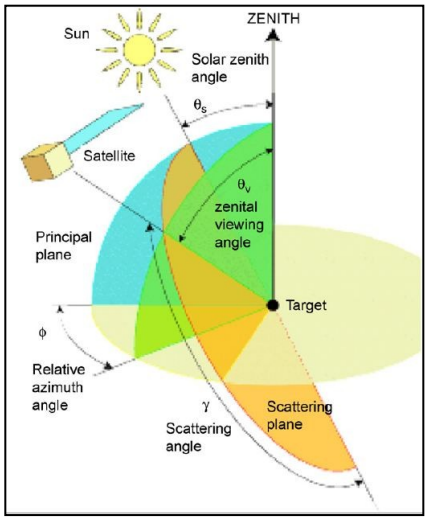


**Figure 1: BRDF view and illumination angle geometry. The positions of the imager and the sun relatively to the target are conventionally represented by three angles known as the zenith viewing angle ($\Theta_v$), the solar zenith angle ($\Theta_s$) and the relative azimuth angle ($_\varphi$). The angle between the incident and scattered directions is called the scattering angle ($\Upsilon$). Image retrieved from http://smsc.cnes.fr/POLDER/lien3_instr.htm on August 19, 2012.**

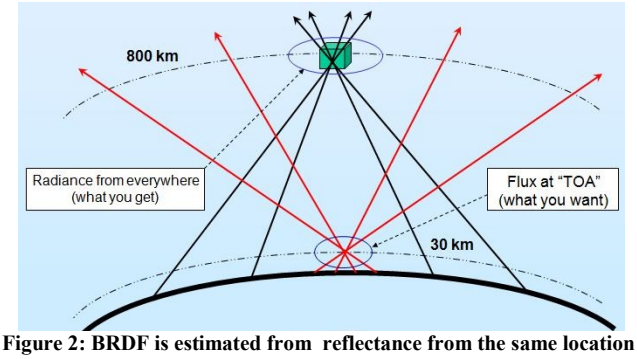


**Figure 2: BRDF is estimated from reflectance from the same location in different angles while a single satellite measures reflectance from different locations. Therefore, the need for multiple satellites for BRDF measurements.**

Existing spaceborne measurements for estimating BRDF, although global, have gaps in at least one or more important requirements for a full BRDF estimation. The angular spread of data points for most instruments even over a full repeat cycle have not been able to image the angular spread of possible anisotropy. MODIS [8] has a period of 100 minutes, however to make a triplet measurement i.e. 3 angular measurements, which is the minimum that any BRDF model needs will take at least 4 hours because the measurements are cross-track, which may be too long a period to study vast-varying tropical clouds or other tropical phenomena. The newer instruments such as the CHRIS [9] and POLDER [10] have achieve angular spread but at the cost of global coverage or spatial resolution. As a result, even with high masses and costs, they have missed out on many scientific interpretations that airborne instruments e.g. CAR have been able to make. However, airborne instruments can only make measurements locally for specific areas and temporally concentrated over a few hours or days. They cannot capture variability in atmospheres over continents over the scale of, say, hurricane development i.e. 1-2 days and the cost per unit area per unit time is very large.

Finally, all the instruments mentioned in this section are nearing their end of life, in fact, Terra carrying MODIS and MISR has already overshot its life by 6 years. With the exception of the NPOESS satellites that will carry the VIIRS sensor – already under testing on the NPP satellites - capable of multi-angular imaging by virtue of its large swath and the CERES instrument, there are no large scale BRDF projects in the pipeline. Due to programmatic changes, NPOESS will likely not be operational before 2017, if not later. This shows a large gap in measurements after the current generation of instruments die out and the newer ones come in.

Nanosatellite clusters and constellations capable of performing high resolution readiometric imaging at a multiple angles and bands and also capable of providing global, temporal coverage is therefore key to filling the gap in BRDF estimations using existing spaceborne or airborne platforms More importantly, they are indispensible for filling the gap of generation

transitions between large instruments because of their low cost, high risk adaptability and low time of development. The next section will describe the low-fuel, formation flight techniques that can be used for BRDF-related measurements and the subsequent sections will describe how these schemes can be adapted for global coverage and the technical feasibility to support the same.

## 3. Mission Implementation: Cluster Formation Flight

Relative motion between any two spacecraft, and can be extended to multiple, is governed by the Hill Clohessy and Wiltshire equations, simplified to be known as the Hill's equations [11]. One satellite is assumed to be traveling in a circular Keplerian orbit while the others are perturbed from this orbit by a small quantity compared to the height of the orbit. The 3D accelerations for any satellite with respect to the origin centered at the first satellite, X axis pointing radially up and away from the earth and Y axis in the direction of orbital motion, is given by:

$$a_x = \ddot{x} - 3n^2x - 2n\dot{y}$$
$$a_y = \ddot{y} + 2n\dot{x}$$
$$a_z = \ddot{z} + n^2z$$

**Equation 1**

By setting the acceleration terms in Equation 1 to 0, we obtain the closed solutions to the Hill's equations i.e. relative geometries which do not need any active control to keep them intact. The analytical closed solution takes the following form with 6 initial conditions:

$$x(t) = \frac{\dot{x_0}}{n}\sin nt - \frac{3x_0 + 2\dot{y_0}}{n}\cos nt + 4x_0 + \frac{2\dot{y_0}}{n}$$
$$y(t) = \frac{2\dot{x_0}}{n}\cos nt + \frac{6x_0 + 4\dot{y_0}}{n}\sin nt - (6nx_0 + 3\dot{y_0})\dot{t} - \frac{2\dot{x_0}}{n} + y_0$$
$$z(t) = \frac{\dot{z_0}}{n}\sin nt + z_0\cos nt$$

**Equation 2**

It can be seen that the x (zenith nadir) and y (along track) motions are coupled but the cross track/z motion is decoupled from both – elliptical motion. To avoid secular growth in relative motion, we can set the secular term to zero ($6nx_0 + 3\dot{y_0} = 0$) in the second equation of Equation 2. The other 5 initial conditions may be tweaked to produce the kind of relative motion desired. For example the offset in y ($y_0$) can be tweaked to produce an in plane formation of a train of satellites like the A-Train. Discussed below are some closed solutions which can be used to make multi-angular BRDF measurements, obtained by closed form solutions of the Hill's equations i.e. no fuel needed to maintain relative configuration.

### 3.1. String of Pearls

In this configuration, the satellites remain in a string in the along track direction separated by a constant distance, say S km. The relative equations of motion for the k'th satellite are given by: $x_k(t) = 0$, $y_k(t) = kS$ and $z_k(t) = 0$. The string of pearls (SOP) cluster formation can recreate MISR-like measurements because it is possible to position 9 nanosatellites that are looking at the same ground spot at the following zenith angles : {-70.5 ; -60.0 ; -45.6 ; - 26.1000 ; 0 ; 26.1000 ; 45.6000 ; 60.0000 ; 70.5000} [12]. The relative geometry is shown as blue and yellow objects (satellites) in Figure 3, where all the satellites point their sensors toward the nadir spot on the ground located at (0,0,-h) in the HCW frame where h is the orbit altitude. Note that the zenith angles with respect to nadir (orange star) at the satellite, i.e. boresight angles, are ***smaller*** than the corresponding angles that the satellite subtends at the orange star with respect to zenith, i.e. view zenith angles, due to Earth's curvature.

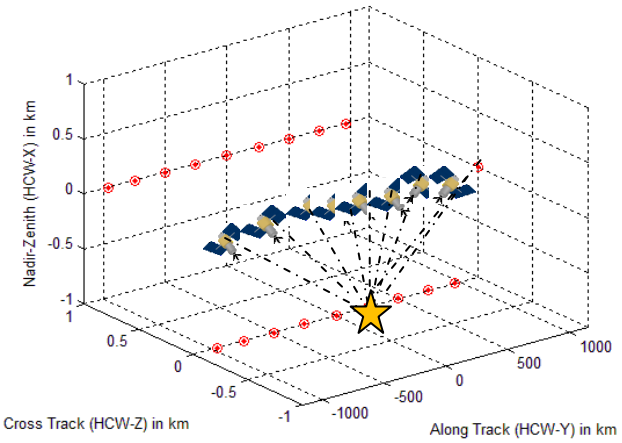


**Figure 3: String of Pearls configuration of a nanosatellite cluster to re-create MISR angles. The blue and yellow objects represent individual satellites, red dots represent the projection of their trajectories on each planes perpendicular to the 2 HCW axes. The nadir-zenith direction has been normalized [-1 1] and is not to scale, the orange star represents the target - point on the ground directly below the LVLH origin.**

While this configuration increases the chances of plume impingement, it reduces the chances of line of sight obstruction. It is the simplest solution for the HCW equations for multiple satellites. The satellites are at the following distances from the HCW origin along the Y-Axis = { -960.2km -746.25km -503.46km -258.4km 0km 258.4km 503.46km 746.25km 960.2km }.

### 3.2. Cross Track Scan

Since the X and Y motion in the HCW frame are uncoupled from the Z motion, the Sop configuration can be extended to include oscillations in the Z direction of any amplitude and phase desired. The frequency will be at the orbital angular rate. The relative equations of motion for the k'th satellite are given by: : $x_k(t) = 0$, $y_k(t) = kS$ and $z_k(t) = z_0\cos(nt + \emptyset)$. $z_0$ and $\emptyset$ can be adjusted for any amplitude and phase, as per BRDF requirements or collision avoidance. For example, $\emptyset = (-1)^k\pi$ will case the satellites to oscillate 180 degrees out of phase with each other and minimize the risk of collision

among consecutive tracks.

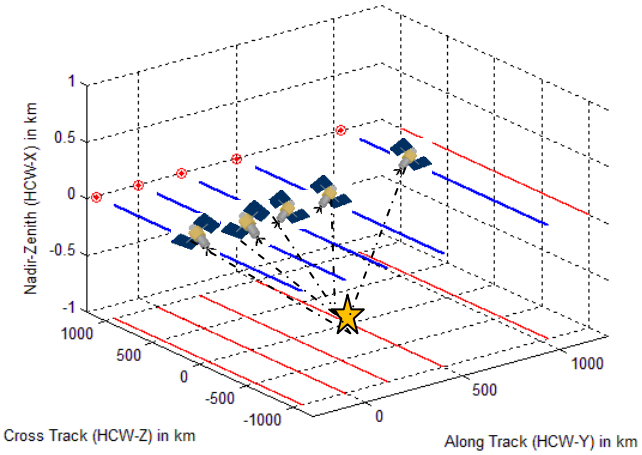


**Figure 4: Cross Track Scan configuration of a nanosatellite cluster (yellow and blue objects), their trajectories in the HCW frame centered at (0,0,0) (blue lines) and the projections in 3 perpendicular planes (red lines/dots). The second satellite from the left periodically crosses the origin. The nadir-zenith direction has been normalized [-1 1] and is not to scale. The orange star represents the target and the dashed black lines the LOS to target.**

Figure 4 shows a cross track scan configuration for a cluster of 5 satellites that project the following boresight angles to target when positioned along the orbit, i.e. along the Y axis : -20°, 0°, 20°, 40°, 60°. As the satellites oscillate about the Y-axis, the boresight changes periodically as does the relative azimuth to the Y-axis as seen in Figure 5 and Figure 6 respectively for $z_0$ = 1000km and Ø= 0. Each satellite starts at the Y-axis, goes to one extreme then to the other extreme and then returns. Note that although $z_0$ and Ø have been kept constant in the simulations shown, they can be varied to suit angles required. The azimuthal angle here in the LVLH or HSW frame is not the solar azimuth as shown on the BRDF plane – that would depend on the orientation of the orbit with respect to the sun in the global frame. The plots have been restricted to show angular variations for satellite lines of sight at >5° elevation, i.e. satellites considered only until 5° at the horizon, therefore restricting the maximum boresight angle that can be reached for line of sight (LOS) to nadir. In Figure 5 and Figure 6, the purple curve representing the rightmost satellite in Figure 4, which subtends the maximum boresight angle among all, has been truncated at positions of the orbit where the satellites subtend the maximum boresight angle i.e. at $z \sim z_0$. Figure 5 has only four curves since the 1st (blue curve) and 3rd (red curve) satellite from the left have motions that are mirror images on the y=0 plane and this exactly same zenith motion and antisymmetric azimuthal motion (Figure 6). The green curve in Figure 6 is a step function because it represents the 2nd satellite from the left whose motion is restricted to y=0 from where the azimuth is measured.

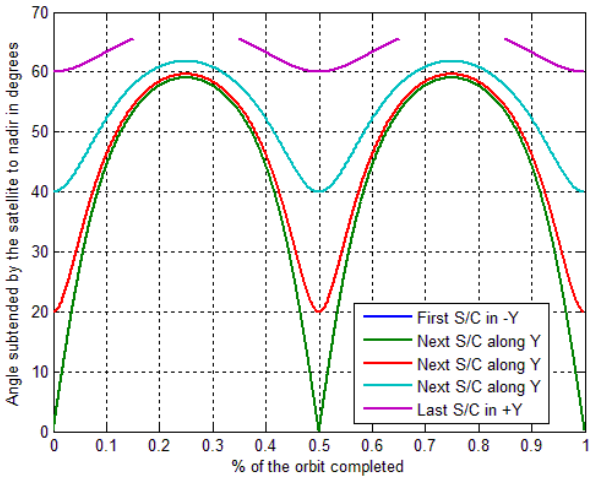


**Figure 5: Variation of boresight or sensor viewing angle at nadir (orange star in Figure 4 representing the target) by the 5 satellites over one orbit for $z_0$ = 1000km and Ø= 0 for all. The leftmost satellite is called 'First S/C in -Y'.**

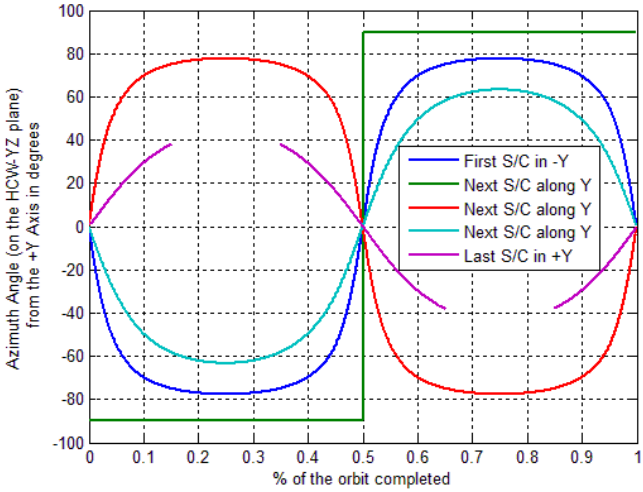


**Figure 6: Variation of azimuth of the 5 satellites in Figure 4, as measured on the YZ plane (LVLH frame) from Y, over one orbit for $z_0$ = 1000km and Ø= 0 for all. The leftmost satellite is called 'First S/C in -Y'.**

### 3.3. Free Orbit Ellipse

The free orbit ellipse configuration has all the satellites arranged in elliptical rings around the LVLH origin. This configuration allows us to achieve both circular rings (at an angle of +/-26.565° to the horizontal) as well as elliptical rings that have circular projections on the ground/x=0 plane (at an angle of +/-30° to the horizontal) [13]. This configuration has been studied in great detail over the last decade to generate synthetic apertures using distributed space systems [14], a topic of interest to the USAF. For a ring formation that projects a circle on the ground [1513], the ellipse of relative motion must project a circle in the along track – cross track plane i.e. $y^2$ +

$z^2 = r^2$, for a projected circle of radius r must always hold. If the initial conditions in Equation 2 are chosen such that: $y_0 = \dot{-}2nx_0$, $y_0 = 2\dot{x_0}/n$, $z_0 = \pm 2x_0$ and $\dot{z_0} = \pm 2\dot{x_0}$, then the Hill's Equations reduce to the following equations and a projected circle of radius as a function of initial x position and velocity only. It can be seen that the condition of the HCW equations that the x:y motion should always trace a 1:2 ellipse in the z=0 plane has been maintained. It is the mutual ratio with the z motion that has projected the circle. The corresponding ellipse has a semi major axis of length $\frac{\sqrt{5}}{2}$R where R is the radius of the projected circle.

$$x(t) = \frac{\dot{x_0}}{n}\sin nt + x_0 \cos nt$$
$$y(t) = \frac{2\dot{x_0}}{n}\cos nt - 2x_0 \sin nt$$
$$z(t) = \frac{2\dot{x_0}}{n}\sin nt + 2x_0 \cos nt$$

**Equation 3**

Figure 7 shows the trajectories of 9 nanosatellites in free-elliptical orbits, 3 satellites per ring. The radii of the ellipses have been chosen such that their projected circles on the LVLH x=0 plane form following boresight angles when looking at nadir (orange star): 20°, 40°, 60°. For each ring, the phases have been chosen to be offset by 120°. The height of the orbit is at 600 km. Equation 3 also shows that the phase of the Z motion is decoupled from X and Y, which gives us the liberty to phase out the 3 satellites as required. Figure 8 and shows the variation of the boresight angle for the LOS to ground target for each of the satellites i.e. the sensor viewing angle in BRDF terms. All the curves in the same ring have been plotted in the same color because they are essentially the same shape with a pi/3 offset – which can be varied per convenience. Figure 9 shows the azimuth of the 9 satellites with respect to the Y-axis. Only 3 curves can be seen because the 3 satellites in each ring have the same phase as the corresponding satellites in the other rings. The step jumps are caused sue to the satellites crossing the Y-axis at different times in the orbit. As with the cross track scan configuration, the plots have been restricted to show angular variations for satellite lines of sight at >5° elevation. As expected, the maximum variation of sensor angle is seen in the outermost ring, so much so that the three satellites in the outermost ring can never see the target at once. Since the full formation is broken for nearly half the orbit, the utility of using multiple satellites per ring is clearly seen i.e. when one can't see the target, another can, albeit at a different azimuth. A big disadvantage of using this cluster is that the satellites tend to traverse enormous lengths in altitude, many of which will be unrealistic e.g. Figure 7. Even if the x-variation and chief orbit altitude are adjusted to make a plausible one, as shown later, the large variation will cause different satellites in the cluster to be at very different heights at different locations of the earth causing large differential drag that needs to be corrected for carefully.

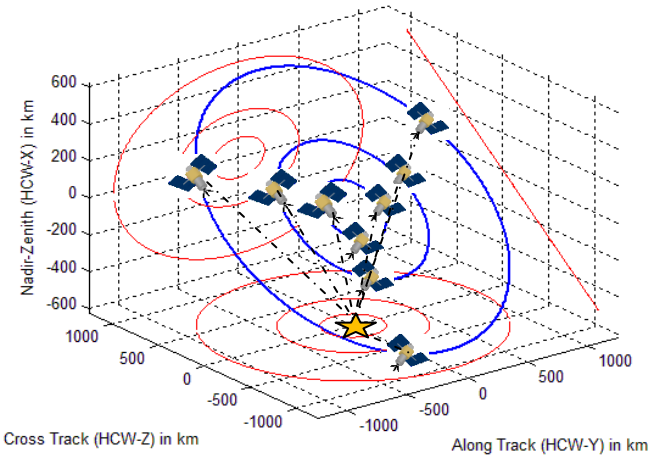


**Figure 7: Free Orbit Ellipse configuration of a nanosatellite cluster (yellow and blue objects), their trajectories in the HCW frame centered at (0,0,0) (blue lines) and the projections in 3 perpendicular planes (red lines). The orange star represents the target – point on the ground directly below the LVLH origin. The dashed lines indicate the satellite line of sight (LOS) to target.**

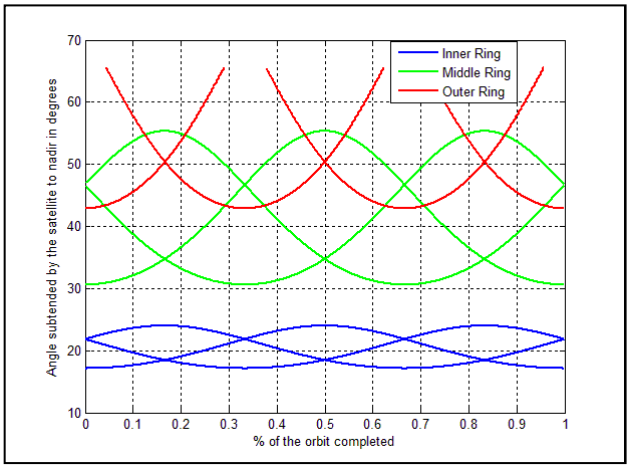


**Figure 8: Variation of boresight or sensor viewing angle at nadir (orange star in Figure 7: the target) by the 9 satellites over one orbit for $z_0 = 2x_0$, i.e. circular projection free elliptical orbit, and 120° apart in phase for each ring**

The Hill's equations show an infinite number of such free orbit ellipses possible for any given radii at specific inclinations to the x=0 plane. For example, in a circular ring, the constraint is: $x^2 + y^2 + z^2 = r^2$ for a circle of radius r for any point in time of the orbit which leads to the following 4 initial conditions for the Hill's equations in Equation 2: $y_0 = \dot{-}2nx_0$, $y_0 = 2\dot{x_0}/n$, $z_0 = \pm\sqrt{3}x_0$ and $\dot{z_0} = \pm\sqrt{3}\dot{x_0}$. Comparing with the elliptical ring with a circular projection, it can be seen that the only difference is the ratio of $x_0/z_0$ which changes from ½ to $1/\sqrt{3}$.

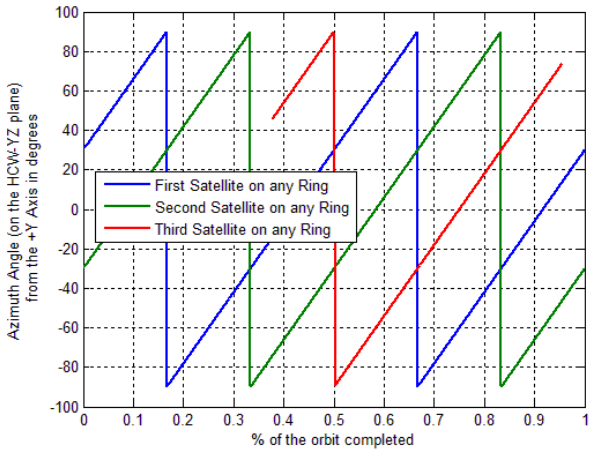


**Figure 9: Variation of azimuth, as measured on the YZ plane (LVLH frame) from Y, by the 9 satellites over one orbit in Figure 7 for $z_0 = 2x_0$, i.e. circular projection free elliptical orbit, and zero phase for all**

## 4. Conclusions

This paper highlights the initial studies for using distributed satellite systems to estimate full and global BRDF. Since BRDF can only be estimated from measurements and not directly measured, its correctness is dependent on the density of angular sampling in the BRDF polar plot for each location, spatial and temporal resolution at that location and number of spectral bands used. Mission literature review showed that no mission is currently capable of estimating full BRDF globally and those are partially doing so right now have less than 5 years of mission life remaining. The paper therefore proposes to use multiple nanosatellites in cluster formation flight and constellations to achieve full, global BRDF estimations. Four zero-fuel cluster geometries have been proposed for circular orbits with no environmental disturbances and their parameters highlighted. Future work includes studying the attitude control system and their influence on ground resolution, methods to initialize the clusters in their relative orbits, effects of disturbance environments (atmospheric drag, J2 perturbations, third body effects, radiation effects) on the cluster components and delta-V and fuel required to achieve this orbit initialization and maintenance. The payload for the mission has not been defined yet and we are currently working with the Optics team to have a candidate ready, capable of multi-spectral imaging in atleast 14 bands over VIS and SWIR, to be inserted into the systems engineering model of the mission.

## 5. References


1. Sandau, R. Status and trends of small satellite missions for Earth observation. *Acta Astronautica* **66**, 1–12 (2010).
2. Kramer, H. J. & Cracknell, A. P. An overview of small satellites in remote sensing*. *International Journal of Remote Sensing* **29**, 4285–4337 (2008).
3. Konecny, G. Small satellites–A tool for Earth observation? *XXth ISPRS Congress, Commission* **4**, 12–23 (2004).
4. Selva, D. & Krejci, D. A survey and assessment of the capabilities of Cubesats for Earth observation. *Acta Astronautica* **74**, 50–68 (2012).
5. Gatebe, C. K. Airborne spectral measurements of surface–atmosphere anisotropy for several surfaces and ecosystems over southern Africa. *Journal of Geophysical Research* **108**, (2003).
6. Román-Colón, M. O. & Strahler, A. H. Land observation from geosynchronous earth orbit (LOGEO): Mission concept and preliminary engineering analysis. *Acta Astronautica* **61**, 101–114 (2007).
7. Esper, J., Neeck, S., Wiscombe, W., Ryschkewitsch, M. & Andary, J. Leonardo-BRDF: A New Generation Satellite Constellation. (2000).at <http://ntrs.nasa.gov/search.jsp?R=20000105058>
8. Xiong, X. *et al.* Terra and Aqua MODIS Design, Radiometry, and Geometry in Support of Land Remote Sensing. *Land Remote Sensing and Global Environmental Change* 133–164 (2011).
9. Barnsley, M. J., Settle, J. J., Cutter, M. A., Lobb, D. R. & Teston, F. The PROBA/CHRIS mission: A low-cost smallsat for hyperspectral multiangle observations of the earth surface and atmosphere. *Geoscience and Remote Sensing, IEEE Transactions on* **42**, 1512–1520 (2004).
10. Deschamps, P. Y. *et al.* The POLDER mission: Instrument characteristics and scientific objectives. *Geoscience and Remote Sensing, IEEE Transactions on* **32**, 598–615 (1994).
11. Hill, G. W. Researches in the lunar theory. *American Journal of Mathematics* **1**, 5–26 (1878).
12. Diner, D. J. *et al.* Multi-angle Imaging SpectroRadiometer (MISR) instrument description and experiment overview. *Geoscience and Remote Sensing, IEEE Transactions on* **36**, 1072–1087 (1998).
13. Sabol, C., Burns, R. & McLaughlin, C. A. Satellite formation flying design and evolution. *Spaceflight mechanics 1999* 265–284 (1999).
14. Kong, E. M. C. Spacecraft formation flight exploiting potential fields. (2002).at <http://ssl.mit.edu/publications/theses/PhD-2002-KongEdmund.pdf>
15. Chichka, D. F. Satellite clusters with constant apparent distribution. *Journal of Guidance, Control, and Dynamics* **24**, (2001).